



Synthesis, Characterization, DFT Studies, Biological Investigation and Molecular Modelling of Novel 1-(5-(1*H*-imidazol-1-yl)-3-methyl-1-phenyl-1*H*-pyrazol-4-yl)-3-amino-2-cyano-*N*-phenyl-1*H*-benzo[*f*]chromene-5-carboxamide Derivatives

RAJAT PATEL^{1,*}, PUJA SHARMA¹, ROHIT R. KOSHTI¹, AKSHAY VYAS¹ and CHETAN B. SANGANI^{2,*}

¹Shri Maneklal M. Patel Institute of Sciences & Research, Kadi Sarva Vishwavidyalaya, Gandhinagar-382024, India

²Department of Chemistry, Government Science College, Sector-15, Gandhinagar-382016, India

*Corresponding authors: E-mail: rajatmsc93@gmail.com; chetansangani1986@yahoo.com

Received: 15 November 2023;

Accepted: 26 December 2023;

Published online: 31 January 2024;

AJC-21523

In this work, a new series of imidazole-pyrazole-benzo[*f*]chromene hybrids were designed and synthesized by a base-catalyzed cyclocondensation through a one-pot multicomponent reaction. All compounds were tested for *in vitro* antimicrobial and anticancer activities. Enzyme inhibitory activities of all compounds were carried out against FabH and EGFR. The majority of synthesized compounds displayed promising antimicrobial as well as anticancer activity against used strains and cancer cell lines respectively. The compounds were also tested for *in vitro* anticancer activities against two cancer cell lines A549 and Hep G2. Compound **7f** (IC₅₀ = 0.62 μM) against EGFR and (IC₅₀ = 1.31 μM) against A549 kinase displayed the most potent inhibitory activity as compared to another member of the series. In the molecular modelling study, compound **7e** was bound into the active pocket of EGFR with one pi-pi interaction and one hydrogen bond having minimum binding energy ΔG_b = -7.6894 kcal/mol. Moreover, FabH molecule **7d** was found to be binding in the active pocket with a minimum binding energy of -8.9117 kcal/mol.

Keywords: Anticancer activity, Imidazole-pyrazole-benzo[*f*]chromene, Enzyme inhibitory activity, One pot multicomponent.

INTRODUCTION

Studies on the discovery of cancer related drugs have made a remarkable progress but still the area needs a lot of research due to less effectiveness and selectivity [1]. It has also been reported that almost 80% of the deaths caused by cancer are related to lung cancer [2]. EGFR is an important class of receptor tyrosine kinase enzyme and considered to be one of the major causes for the substantial growth and survival of tumour cells. Abnormally high EGFR expression and its mutation is considered to be one of the leads to cancer proliferation, increased metastasis potential and neo angiogenesis [3-6]. Mutations in EGFR also is responsible for the increased drug resistance. An effective way to overcome such type of mutations and over-expression EGFR inhibitors play a vital role [7]. Targeted therapy that involves inhibiting EGFR by blocking tyrosine-kinase with inhibitors at the ATP-binding site in the cytoplasmic wall is a unique method to prevent the growth and spread of cancer cells [8].

Nitrogen containing heterocyclic rings play an important role in the field of medicinal chemistry. Due to their multiple uses as active biological scaffolds and their distinct characteristics they are of significant importance in the pharmaceutical field [9-15]. Studies show that pyrazoles and their derivatives are of great importance due to their varied biological activities. Pyrazoles and their derivatives are found to have excellent anticancer [16], antimicrobial [17], anti-inflammatory [18] and analgesic [19] activities. Taking into account the broad spectrum of biological activities of pyrazole ring, it is considered to be a significant moiety to be added in the drug discovery and henceforth in the pharmaceutical sector.

In addition, a number of other pharmacologically active scaffolds like imidazole are also known to be of importance due to their extensive biological activities and application in drug designing. Imidazole and their derivatives also possess pharmacological activities like anti-convulsant [20], anticancer [21], antitubercular [22], antiinflammatory [23] and antimicro-

bial [24]. Both imidazole and pyrazole rings have been a part of a number of drugs in clinical use.

Prompted by these significant bio-profile of pyrazole and imidazole derivatives and their importance in the medicinal field and with the purpose of continuation of research of novel biologically active heterocyclic scaffolds, we clubbed pyrazole and imidazole moieties along with other bioactive moieties into a single target molecule to obtain a novel series of potent bioactive molecule. In present work, a novel series comprising of antimicrobial moieties is synthesized by combining pyrazole and imidazole derivatives along with their biological evaluation for any significant changes and DFT studies and molecular modelling of novel 1-(5-(1*H*-imidazol-1-yl)-3-methyl-1-phenyl-1*H*-pyrazol-4-yl)-3-amino-2-cyano-*N*-phenyl-1*H*-benzo[*f*]chromene-5-carboxamide and its derivatives using one pot MCR approach is reported.

EXPERIMENTAL

All chemicals were purchased commercially and used as such. The FTIR spectral data of all the synthesized compounds were recorded using Perkin-Elmer Spectrum-GX spectrophotometer with KBr pellets. Silica gel coated aluminium plates 60 F₂₅₄, 0.25 mm thickness, Merck were used to check and monitor each step of synthesis. Thermo-Fisher LCMS spectrometer was involved in the determination of mass spectra while ¹H NMR and ¹³C NMR were observed in DMSO-*d*₆ on a Bruker Avance 400 MHz spectrometer with TMS as internal standard and DMSO as solvent. Elemental analysis of all the synthesized compounds were carried out using Perkin-Elmer CHN/S/O Elemental Analyzer 2400 Series II.

Synthesis of target molecule 1-(5-(1*H*-imidazol-1-yl)-3-methyl-1-phenyl-1*H*-pyrazol-4-yl)-3-amino-2-cyano-*N*-phenyl-1*H*-benzo[*f*]chromene-5-carboxamide derivatives (7a-h): The starting compound 3-methyl-1-phenyl-1*H*-pyrazole-5-one (**1a-d**) was prepared as per the literature procedure by refluxing equimolar mixture of ethylacetoacetate and phenyl hydrazine with glacial acetic acid in water bath at 70 °C for 90 min. The mixture was then cooled on a water bath and ether was added slowly with continuous stirring when precipitates of the starting material **1a-d** were separated out. The final product was checked using TLC.

Vilsmeier-Haack reaction (chloroformylation) as per the literature procedure was involved in converting the starting material **1a-d** into 3-methyl-1-phenyl-5-chloro-1*H*-pyrazole-4-carbaldehyde (**2a-d**) by first preparing an iminium salt by mixing ice cold equimolar solutions of POCl₃ and DMF and then refluxing it with 3-methyl-1-phenyl-1*H*-pyrazole-5-one (**1a-d**) for 5 h at 90 °C. The resulting mixture after reaching to room temperature was then poured on crushed ice when 3-methyl-1-phenyl-5-chloro-1*H*-pyrazole-4-carbaldehyde (**2a-d**) separates out. The precipitates were washed with water to remove all acidic impurities and recrystallized with ethanol. The final product was confirmed using TLC.

In next step, the nucleophilic substitution of chloro group in pyrazole by imidazole was carried out by refluxing 3-methyl-1-phenyl-5-chloro-1*H*-pyrazole-4-carbaldehyde (**2a-d**) with imidazole (**3**) for 2 h at 85 °C using DMF as solvent and K₂CO₃

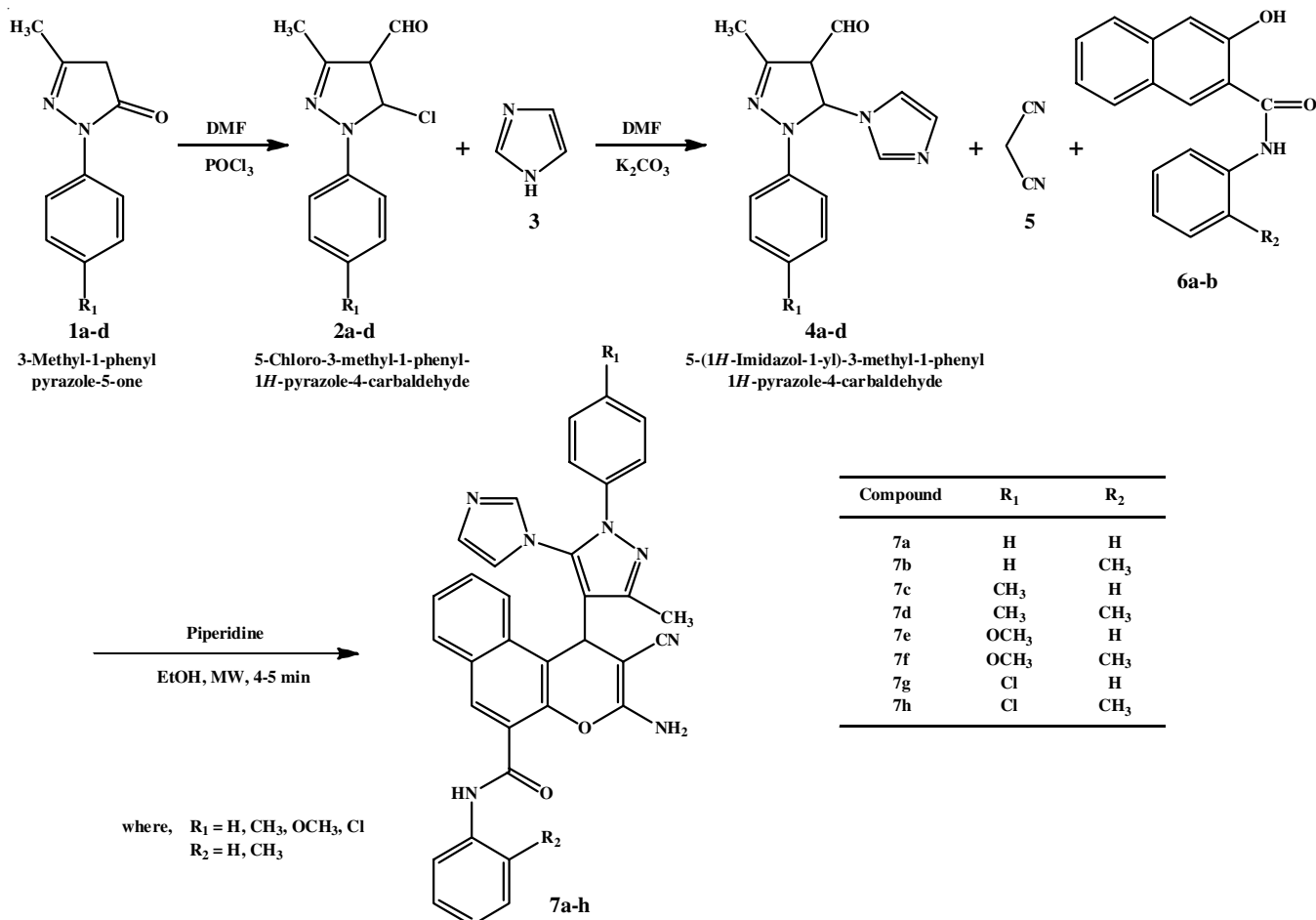
as base catalyst. After the completion of reaction, the reaction mixture was poured on ice cold water when the precipitates of 5-(1*H*-imidazol-1-yl)-3-methyl-1-phenyl-1*H*-pyrazole-4-carbaldehyde (**4a-d**) separate out, which was filtered, washed and recrystallized with ethanol.

The target molecules were then synthesized using the one pot MCR approach. For this, the calculated quantity of 5-(1*H*-imidazol-1-yl)-3-methyl-1-phenyl-1*H*-pyrazole-4-carbaldehyde (**4a-d**), malanonitrile (**5**) and 3-hydroxy-*N*-phenyl-2-naphthamide (**6a-b**) were refluxed for almost 3 h in a round bottom flask. The mixture at room temperature gave the final product 1-(5-(1*H*-imidazol-1-yl)-3-methyl-1-phenyl-1*H*-pyrazol-4-yl)-3-amino-2-cyano-*N*-phenyl-1*H*-benzo[*f*]chromene-5-carboxamide (**7a-h**), which was recrystallized using ethanol and confirmed with TLC (**Scheme-I**).

1-(5-(1*H*-Imidazol-1-yl)-3-methyl-1-phenyl-1*H*-pyrazol-4-yl)-3-amino-2-cyano-*N*-phenyl-1*H*-benzo[*f*]chromene-5-carboxamide (7a): Yield: 78%. IR (KBr, ν_{max}, cm⁻¹): 3450 (N-H *str.*), 3032 (arom. C-H *str.*), 2110 (-CN *str.*), 1670 (C=O *str.* of -NHCO-), 1545 & 1460 (C=C *str.* of aromatic ring), 1234 (C-O-C *str.* of Ar-O), 1280 (-NH₂ *str.*). ¹H NMR (400 MHz, DMSO-*d*₆) δ ppm: 2.03 (s, 3H, CH₃), 4.85 (s, 1H, -CH-), 6.82 (s, 2H, -NH₂), 7.02-8.10 (m, 18H, Ar-H), 9.95 (s, 1H, NH). ¹³C NMR (400 MHz, DMSO-*d*₆) δ in ppm: 14.15 (CH₃), 19.45 (CH), 59.24, 112.21, 119.00, 120.24, 120.24, 121.60, 121.60, 122.32, 123.38, 123.91, 126.22, 126.50, 127.83, 128.00, 128.22, 128.64, 129.00, 129.00, 129.35, 129.35, 129.70, 132.23, 134.05, 134.55, 137.90, 139.65, 147.15, 151.45, 151.60, 177.10 (Ar-C), 117.30 (-CN), 164.72 (C=O). MS (*m/z*): 563.21 (M⁺). Anal. calcd. (found) % for C₃₄H₂₅N₇O₂ (*m.w.* 563.62 g/mol): C, 72.46 (72.36); H, 4.47 (4.34); O, 5.68 (5.81); N, 17.40 (17.23).

1-(5-(1*H*-Imidazol-1-yl)-3-methyl-1-phenyl-1*H*-pyrazol-4-yl)-3-amino-2-cyano-*N*-(*o*-tolyl)-1*H*-benzo[*f*]chromene-5-carboxamide (7b): Yield: 81%. IR (KBr, ν_{max}, cm⁻¹): 3453 (N-H *str.*), 3030 (arom. C-H *str.*), 2114 (-CN *str.*), 1672 (C=O *str.* of -NHCO-), 1546 & 1463 (C=C *str.* of aromatic ring), 1232 (C-O-C *str.* of Ar-O), 1284 (-NH₂ *str.*). ¹H NMR (400 MHz, DMSO-*d*₆) δ ppm: 2.03 (s, 3H, CH₃), 2.24 (s, 3H, CH₃), 4.85 (s, 1H, -CH-), 6.82 (s, 2H, -NH₂), 7.02-8.10 (m, 17H, Ar-H), 9.95 (s, 1H, NH). ¹³C NMR (400 MHz, DMSO-*d*₆) δ in ppm: 14.15 (CH₃), 17.25 (CH₃), 19.45 (CH), 59.24, 112.21, 119.00, 120.24, 120.24, 121.60, 122.32, 123.38, 123.91, 126.22, 126.50, 127.83, 128.00, 128.22, 128.64, 128.90, 130.32, 129.35, 129.35, 129.70, 131.20, 132.23, 134.05, 134.55, 134.72, 139.65, 147.15, 151.45, 151.60, 177.10 (Ar-C), 117.30 (-CN), 164.72 (C=O). MS (*m/z*): 577.22 (M⁺). Anal. calcd. (found) % for C₃₅H₂₇N₇O₂ (*m.w.* 577.65 g/mol): C, 72.78 (72.60); H, 4.71 (4.53); O, 5.54 (5.70); N, 16.97 (16.83).

1-(5-(1*H*-Imidazol-1-yl)-3-methyl-1-(*p*-tolyl)-1*H*-pyrazol-4-yl)-3-amino-2-cyano-*N*-phenyl-1*H*-benzo[*f*]chromene-5-carboxamide (7c): Yield: 83%. IR (KBr, ν_{max}, cm⁻¹): 3455 (N-H *str.*), 3034 (arom. C-H *str.*), 2108 (-CN *str.*), 1668 (C=O *str.* of -NHCO-), 1542 & 1462 (C=C *str.* of aromatic ring), 1230 (C-O-C *str.* of Ar-O), 1282 (-NH₂ *str.*). ¹H NMR (400 MHz, DMSO-*d*₆) δ ppm: 2.03 (s, 3H, CH₃), 2.47 (s, 3H, CH₃), 4.85 (s, 1H, -CH-), 6.82 (s, 2H, -NH₂), 7.02-8.10 (m, 17H, Ar-H), 9.95 (s, 1H, NH). ¹³C NMR (400 MHz, DMSO-*d*₆) δ ppm: 14.15



Scheme-I: Synthetic route of novel 1-(5-(1*H*-imidazol-1-yl)-3-methyl-1-phenyl-1*H*-pyrazol-4-yl)-3-amino-2-cyano-*N*-phenyl-1*H*-benzo[*f*]chromene-5-carboxamide derivatives

(CH₃), 19.45 (CH), 21.30 (CH₃), 59.24, 112.21, 119.00, 120.24, 120.24, 121.60, 122.32, 123.38, 123.91, 126.22, 126.50, 127.83, 128.00, 128.22, 128.64, 128.90, 130.32, 129.35, 129.35, 129.70, 131.20, 132.23, 134.05, 134.55, 134.72, 139.65, 147.15, 151.45, 151.60, 177.10 (Ar-C), 117.30 (-CN), 164.72 (C=O). MS (*m/z*): 577.22 (M⁺). Anal. calcd. (found) % for C₃₅H₂₇N₇O₂ (*m.w.* 577.65 g/mol): C, 72.78 (72.60); H, 4.71 (4.53); O, 5.54 (5.70); N, 16.97 (16.83).

1-(5-(1*H*-Imidazol-1-yl)-3-methyl-1-(*p*-tolyl)-1*H*-pyrazol-4-yl)-3-amino-2-cyano-*N*-(*o*-tolyl)-1*H*-benzo[*f*]chromene-5-carboxamide (7d): Yield: 77%. IR (KBr, ν_{max} , cm⁻¹): 3451 (N-H *str.*), 3032 (arom. C-H *str.*), 2115 (-CN *str.*), 1675 (C=O *str.* of -NHCO-), 1545 & 1463 (C=C *str.* of aromatic ring), 1230 (C-O-C *str.* of Ar-O), 1278 (-NH₂ *str.*). ¹H NMR (400 MHz, DMSO-*d*₆) δ ppm: 2.03 (s, 3H, CH₃), 2.24 (s, 3H, CH₃), 2.47 (s, 3H, CH₃), 4.85 (s, 1H, -CH-), 6.82 (s, 2H, -NH₂), 7.00-7.90 (m, 16H, Ar-H), 9.97 (s, 1H, NH). ¹³C NMR (400 MHz, DMSO-*d*₆) δ ppm: 14.15 (CH₃), 17.25 (CH₃), 19.45 (CH), 21.30 (CH₃), 59.24, 112.21, 119.00, 120.24, 120.24, 121.60, 121.60, 122.32, 123.38, 123.91, 126.50, 127.83, 128.00, 128.22, 128.64, 129.00, 129.00, 129.35, 129.35, 129.70, 132.23, 134.05, 134.55, 135.61, 137.90, 139.65, 147.15, 151.45, 151.60, 177.10 (Ar-C), 117.30 (-CN), 164.72 (C=O). MS (*m/z*): 591.24 (M⁺). Anal. calcd. (found) % for C₃₆H₂₉N₇O₂ (*m.w.* 591.68 g/mol): C, 73.08 (73.20); H, 4.94 (5.12); O, 5.41 (5.34); N, 16.57 (16.71).

1-(5-(1*H*-Imidazol-1-yl)-1-(4-methoxyphenyl)-3-methyl-1*H*-pyrazol-4-yl)-3-amino-2-cyano-*N*-phenyl-1*H*-benzo[*f*]chromene-5-carboxamide (7e): Yield: 80%. IR (KBr, ν_{max} , cm⁻¹): 3452 (N-H *str.*), 3035 (arom. C-H *str.*), 2115 (-CN *str.*), 1673 (C=O *str.* of -NHCO-), 1546 & 1462 (C=C *str.* of aromatic ring), 1232 (C-O-C *str.* of Ar-O), 1285 (-NH₂ *str.*), 1255 (C-O *str.* alkylaryl ether). ¹H NMR (400 MHz, DMSO-*d*₆) δ ppm: 2.03 (s, 3H, CH₃), 3.75 (s, 3H, OCH₃), 4.85 (s, 1H, -CH-), 6.82 (s, 2H, -NH₂), 7.02-8.10 (m, 17H, Ar-H), 9.95 (s, 1H, NH). ¹³C NMR (400 MHz, DMSO-*d*₆) δ ppm: 14.15 (CH₃), 19.45 (CH), 55.80 (OCH₃), 59.24, 112.21, 112.21, 114.90, 114.90, 119.00, 120.24, 120.24, 121.60, 121.60, 122.32, 123.38, 123.91, 126.22, 126.50, 127.83, 128.00, 128.22, 128.64, 129.00, 129.00, 129.70, 132.23, 134.05, 134.55, 137.90, 139.65, 151.45, 151.60, 177.10 (Ar-C), 117.30 (-CN), 164.72 (C=O). MS (*m/z*): 593.22 (M⁺). Anal. calcd. (found) % for C₃₅H₂₇N₇O₃ (*m.w.* 593.65 g/mol): C, 70.81 (70.96); H, 4.58 (4.71); O, 8.09 (7.94); N, 16.52 (16.43).

1-(5-(1*H*-Imidazol-1-yl)-1-(4-methoxyphenyl)-3-methyl-1*H*-pyrazol-4-yl)-3-amino-2-cyano-*N*-(*o*-tolyl)-1*H*-benzo[*f*]chromene-5-carboxamide (7f): Yield: 77%. IR (KBr, ν_{max} , cm⁻¹): 3450 (N-H *str.*), 3031 (arom. C-H *str.*), 2108 (-CN *str.*), 1675 (C=O *str.* of -NHCO-), 1542 & 1465 (C=C *str.* of aromatic ring), 1230 (C-O-C *str.* of Ar-O), 1281 (-NH₂ *str.*), 1251 (C-O *str.* alkylaryl ether). ¹H NMR (400 MHz, DMSO-

d_6) δ ppm: 2.03 (s, 3H, CH₃), 2.24 (s, 3H, CH₃), 3.75 (s, 3H, OCH₃), 4.85 (s, 1H, -CH-), 6.82 (s, 2H, -NH₂), 6.95-8.03 (m, 16H, Ar-H), 9.95 (s, 1H, NH). ¹³C NMR (400 MHz, DMSO-*d*₆) δ ppm: 14.15 (CH₃), 17.25 (CH₃), 19.45 (CH), 55.80 (OCH₃), 59.24, 112.21, 112.21, 114.90, 114.90, 119.00, 120.24, 120.24, 121.60, 121.60, 122.32, 123.38, 123.91, 126.22, 126.50, 127.83, 128.00, 128.22, 128.64, 129.12, 129.12, 129.70, 132.23, 133.10, 134.55, 137.45, 139.65, 151.30, 151.71, 177.10 (Ar-C), 117.30 (-CN), 164.72 (C=O). MS (*m/z*): 607.23 (M⁺). Anal. calcd. (found) % for C₃₆H₂₉N₇O₃ (*m.w.* 607.67 g/mol): C, 71.16 (71.29); H, 4.81 (4.68); O, 7.90 (8.06); N, 16.14 (16.26).

3-Amino-1-(1-(4-chlorophenyl)-5-(1H-imidazol-1-yl)-3-methyl-1H-pyrazol-4-yl)-2-cyano-N-phenyl-1H-benzof[*f*]-chromene-5-carboxamide (7g): Yield: 75%; IR (KBr, ν_{\max} , cm⁻¹): 3450 (N-H *str.*), 3030 (arom. C-H *str.*), 2110 (-CN *str.*), 1673 (C=O *str.* of -NHCO-), 1545 & 1460 (C=C *str.* of aromatic ring), 1231 (C-O-C *str.* of Ar-O), 1282 (-NH₂ *str.*), 770 (-Cl *str.*). ¹H NMR (400 MHz, DMSO-*d*₆) δ ppm: 2.03 (s, 3H, CH₃), 4.85 (s, 1H, -CH-), 6.82 (s, 2H, -NH₂), 7.02-8.10 (m, 17H, Ar-H), 9.95 (s, 1H, NH). ¹³C NMR (400 MHz, DMSO-*d*₆) δ ppm: 14.15 (CH₃), 19.45 (CH), 59.24, 112.21, 119.00, 120.24, 120.24, 121.60, 121.60, 122.32, 123.38, 123.91, 126.22, 126.50, 127.83, 128.00, 128.22, 128.64, 129.00, 129.00, 129.35, 129.35, 129.70, 132.23, 134.05, 134.55, 137.90, 139.65, 147.15, 151.45, 151.60, 177.10 (Ar-C), 117.30 (-CN), 164.72 (C=O). MS (*m/z*): 597.17 (M⁺). Anal. calcd. (found) % for C₃₄H₂₄N₇O₂Cl (*m.w.* 598.06 g/mol): C, 68.28 (68.10); H, 4.05 (4.21); O, 5.35 (5.23); N, 16.39 (16.43); Cl, 5.93 (6.07).

3-Amino-1-(1-(4-chlorophenyl)-5-(1H-imidazol-1-yl)-3-methyl-1H-pyrazol-4-yl)-2-cyano-N-(*o*-tolyl)-1H-benzof[*f*]-chromene-5-carboxamide (7h): Yield: 77%. IR (KBr, ν_{\max} , cm⁻¹): 3452 (N-H *str.*), 3035 (arom. C-H *str.*), 2114 (-CN *str.*), 1670 (C=O *str.* of -NHCO-), 1545 & 1463 (C=C *str.* of aromatic ring), 1230 (C-O-C *str.* of Ar-O), 1285 (-NH₂ *str.*), 775 (-Cl *str.*). ¹H NMR (400 MHz, DMSO-*d*₆) δ ppm: 2.03 (s, 3H, CH₃), 2.24 (s, 3H, CH₃), 4.85 (s, 1H, -CH-), 6.82 (s, 2H, -NH₂), 7.00-7.90 (m, 16H, Ar-H), 9.97 (s, 1H, NH). ¹³C NMR (400 MHz, DMSO-*d*₆) δ ppm: 14.15 (CH₃), 17.25 (CH₃), 19.45 (CH), 59.24, 112.21, 119.00, 120.24, 120.24, 121.60, 122.32, 123.38, 123.91, 126.22, 126.50, 127.83, 128.00, 128.22, 128.64, 128.90, 130.32, 129.35, 129.35, 129.70, 131.20, 132.23, 134.05, 134.55, 134.72, 139.65, 147.15, 151.45, 151.60, 177.10 (Ar-C), 117.30 (-CN), 164.72 (C=O). MS (*m/z*): 611.18 (M⁺). Anal. calcd. (found) % for C₃₅H₂₆N₇O₂Cl (*m.w.* 612.09 g/mol): C, 68.68 (68.81); H, 4.28 (4.37); O, 5.23 (5.13); N, 16.02 (15.91); Cl, 5.79 (5.92).

RESULTS AND DISCUSSION

Infrared spectra studies: All the eight synthesized compounds **7a-h** were subjected to IR spectral analysis to confirm the different functional groups present in them. The stretching frequency of compounds **7a-h** for -NH group was observed in the range of 3455-3450 cm⁻¹ while the aromatic C-H stretching was observed at 3035-3030 cm⁻¹ and for C=C stretching the IR spectral range was observed at 1546-1542 and 1465-1460 cm⁻¹. Stretching bands for the -CN was observed in the range of 2115-2108 cm⁻¹ and for -NHCO in the spectral range of 1675-1668 cm⁻¹ for all the synthesized compounds.

All compounds gave IR spectra for C-O-C ether linkage of Ar-O from 1234-1230 cm⁻¹ and for -NH₂ group the range was 1285-1278 cm⁻¹. Alkyl aryl ether linkage C-O for compounds **7e** and **7f** was observed at 1255-1251 cm⁻¹ and a C-Cl stretching for compounds **7g** and **7h** appeared in the range of 775 cm⁻¹.

¹H NMR spectral studies: The ¹H NMR spectra of the synthesized compounds **7a-h** indicated a singlet for three protons of a methyl group appeared at δ 2.03 ppm whereas in compounds **7c** and **7d**, a singlet for three protons for methyl group as R₁ substitution was observed at δ 2.47 ppm. A singlet for three protons of methyl group as R₂ substitution in compounds **7b**, **7d**, **7f** and **7g** was observed at δ 2.24 ppm. A singlet for an aromatic chiral proton for all eight synthesized compounds **7a-h** indicating the cyclization of final product appeared in the range of δ 4.85 ppm. In compounds **7e** and **7f**, singlet for three protons of methoxy group as R₁ substitution appeared at δ 3.75 ppm. All compounds **7a-h** gave a singlet stretching for two protons of amine -NH₂ in the region of δ 6.82 ppm and a singlet for single proton of -NH group at δ 9.95 ppm. A multiplet for aromatic protons from sixteen to eighteen appeared in the range of δ 7.02-8.10 ppm for all the eight synthesized compounds.

¹³C NMR spectral studies: All the eight synthesized compounds **7a-h** showed signals in the region of δ 14.15 ppm for -CH₃ group. Methyl group as R₁ substitution in compounds **7c**, **7d** appeared in the range of δ 21.30 ppm whereas as R₂ substitution in compounds **7b**, **7d**, **7f**, **7h** appeared at δ 17.25 ppm. The methoxy group as R₁ substitution in compounds **7e**, **7f** was found in the range of δ 55.80 ppm. Active methylene C4 (-CH) for compounds **7a-h** showed a single line at δ 19.45 ppm. The synthesized compounds also exhibited a single peak at δ 117.30 ppm for cyanide (-CN) group and a single peak at δ 164.72 ppm for the carbonyl (-C=O) group. A multiplet of aromatic carbon atoms in all compounds was confirmed in the range of δ 59.24-177.10 ppm.

Biological evaluation

Antiproliferation and EGFR inhibitory activity: Eight new compounds with substituted imidazole, pyrazol and substituted *N*-phenyl benzo[*f*]chromenecarboxamide were synthesized tested for EGFR inhibitory activity as well as anti-proliferation activity against known lung cancer cell line A549 known as adenocarcinoma human alveolar basal epithelial cell line and liver cancer cell line Hep G2, where the results obtained from this study is represented in Table-1. The inhibition of EGFR and its mode of action is known by stopping the transferring of signal between the two EGFR molecules. On testing the activities and effectiveness of these molecules, it was found that compound **7f** showed most potent activity amongst the prepared compounds with IC₅₀ of 0.62 ± 0.02 μM, while compounds **7h** and **7e** showed compared good activity with IC₅₀ of 0.66 ± 0.03 μM and IC₅₀ of 0.78 ± 0.03 μM, respectively. In the case of anti-proliferative activity against A549, compounds **7h** and **7f** showed most potent activity with IC₅₀ of 1.24 ± 0.05 μM and 1.31 ± 0.03 μM, respectively, while for Hep G2 compounds **7f** and **7e** showed most potent activity with IC₅₀ of 1.36 ± 0.03 μM and 1.84 ± 0.03 μM, respectively. Although

TABLE-1
INHIBITION OF EGFR KINASE AND ANTIPROLIFERATIVE
ACTIVITY IC₅₀ (μM) OF COMPOUNDS 7a-h

Compd.	EGFR	A549	Hep G2
7a	12.23 ± 0.04	16.25 ± 0.02	18.23 ± 0.06
7b	11.79 ± 0.04	19.54 ± 0.02	17.54 ± 0.05
7c	4.26 ± 0.05	5.24 ± 0.06	7.29 ± 0.03
7d	3.69 ± 0.03	3.53 ± 0.04	4.17 ± 0.06
7e	0.78 ± 0.03	1.98 ± 0.04	1.84 ± 0.03
7f	0.62 ± 0.02	1.31 ± 0.03	1.36 ± 0.03
7g	10.12 ± 0.05	9.84 ± 0.06	11.21 ± 0.07
7h	0.66 ± 0.03	1.24 ± 0.05	2.02 ± 0.04
Erlotinib	0.032 ± 0.02	0.13 ± 0.01	0.12

among all the synthesized compounds only compounds 7f and 7e showed the nearest potency compared to standard erlotinib.

***E. coli* FabH inhibitory activity:** Synthesized eight compounds 7a-h with various substitution were examined for the *E. coli* FabH inhibitory activity and the results obtained from this study is represented in Table-2, the inhibition concentration is represented in micromole. Among these eight examined compounds, three showed a decent inhibitory activity. Compound 7h showed the most potent inhibitory activity with the IC₅₀ of 2.7 μM, while compound 7d showed inhibitory action at the IC₅₀ of 3.4 μM and compound 7f showed inhibitory action at the IC₅₀ of 3.8 μM. While the other derivatives 7a, 7b, 7c, 7e and 7g showed relatively very low and poor inhibitory action at the IC₅₀ of 13.6 μM, 18.2 μM, 6.8 μM, 12.6 μM and 11.6 μM, respectively.

TABLE-2
E. coli FabH INHIBITORY ACTIVITY OF
SYNTHESIZED COMPOUNDS 7a-h

Compd.	R ₁	R ₂	<i>E. coli</i> FabH IC ₅₀ (μM)	Hemolysis LC30 ^a (mg/mL)
7a	H	H	13.6	> 10
7b	H	CH ₃	18.2	> 10
7c	CH ₃	H	6.8	> 10
7d	CH ₃	CH ₃	3.4	> 10
7e	OCH ₃	H	12.9	> 10
7f	OCH ₃	CH ₃	3.8	> 10
7g	Cl	H	11.6	> 10
7h	Cl	CH ₃	2.7	> 10

Lytic concentration 30%

Molecular docking study

With EGFR: The synthesized compounds 7a-h interacted with the active pocket of the protein of EGFR by using the molecular docking method, to study the pharmacophore with various substitutions allowing better fitting into the active pocket and guiding the SAR. The homology model of all compounds with the protein PDB file of active pocket of EGFR protein was corrected using MOE software and; missing fragments and assigning partial charge were assigned to the prepared module. The lowest energy homology model of the geometrically optimized ligand structure was used to dock the ligand site with rigorous receptor refinement. Table-3 shows the resultant binding energy of all docked molecules. From the all synthesized compounds, it was concluded that the main interaction observed

TABLE-3
BINDING ENERGY OF COMPOUNDS 7a-h WITH EGFR

Compd.	R ₁	R ₂	Binding energy (ΔGb)
7a	H	H	-7.3289
7b	H	CH ₃	-6.6029
7c	CH ₃	H	-7.3439
7d	CH ₃	CH ₃	-7.2507
7e	OCH ₃	H	-7.6894
7f	OCH ₃	CH ₃	-7.5749
7g	Cl	H	-7.2586
7h	Cl	CH ₃	-7.6125

by compound 7e is one pi-pi interaction between the methoxy phenyl ring with Trp 32 and, one hydrogen bond between the phenylamine ring with Asn 247. Compound 7e was bound into the active site of the EGFR pocket with the minimum binding energy of ΔGb = - 7.6894 kcal/mol, amongst the all docked. Figs. 1 and 2 show 2D and 3D binding interaction with the pocket boundary and pocket cavity, respectively with all the amino acids of EGFR protein residues labelled with their short-code within the radius of 4.08 Å of the ligand atom. The binding energy of compound 7e and EGFR are shown in which two types of interaction present on of the hydrophobic and aromatic interactions. The binding was stabilized by one pi-pi interaction between Trp 32 and the methoxy phenyl ring adjacent to the

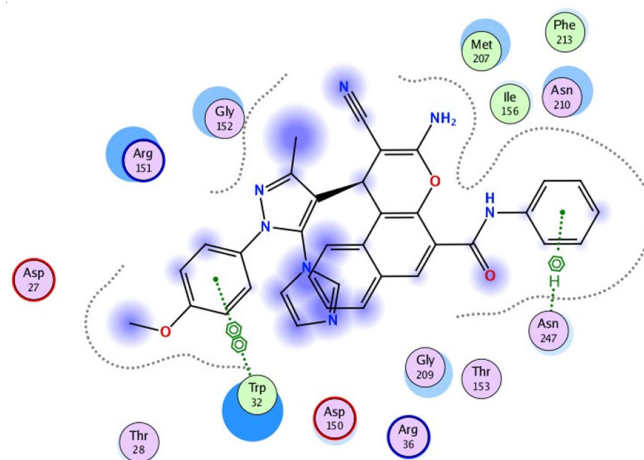


Fig. 1. 2D Binding model of compound 7e into the active pocket of EGFR

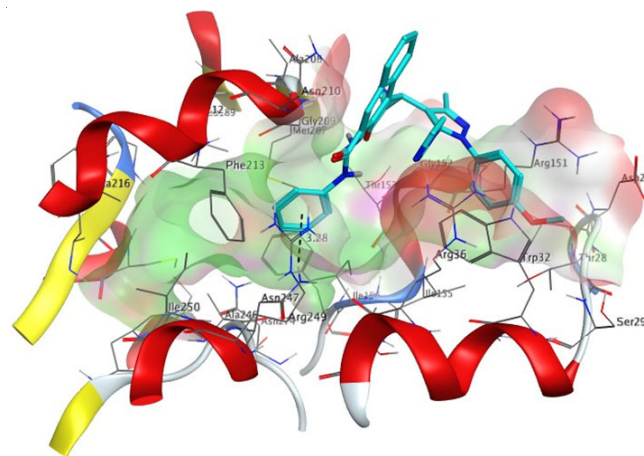


Fig. 2. 3D Binding model of compound 7e into the active pocket of EGFR

pyrazole ring with a bond distance of 3.28 Å and one hydrogen bond between the phenylamine rings with Asn 247 with a bond distance of 3.21 Å in the form of arene hydrogen interaction. From this binding model, it could be concluded that these pi-pi interaction and hydrogen bonds from the methoxy phenyl ring and phenylamine rings with the pocket can be said to be responsible for the effective EGFR inhibitory of compound **7e** from the docking results.

With FabH: Similarly, the synthesized compounds **7a-h** and *E. coli* FabH interacted with the active pocket of the protein of *E. coli* FabH-CoA complex structure (PDB code: 1HNJ) by using the molecular docking method and to understand the behaviour of the pharmacophore with various substitutions allowing better fitting into the active pocket and to guide the SAR. A catalytic triad tunnel composed of Cys-His-Asn is found in the active site of FabH, which is found in many bacteria. This triad works as catalysis plays an important role in the controlling of chain elongation as well as substrate binding and hence the alkyl chain of CoA is broken at the Cys residue of the triad of FabH, the interaction occurring between the Cys and substrate seems to play a significant role in the binding of the substrate. The lowest energy homology model of the geometrically optimized ligand structure was used to dock the ligand site with rigorous receptor refinement. The binding energy data of all docked molecules is represented in Table-4. The binding efficiency of all synthesized compounds **7a-h** was studied after concluding that compound **7d** was found to be bound strongly into the active pocket of the FabH with one pi-pi interaction, two hydrogen bonds and one cation-pi interaction, the binding energy ΔG_b of -8.9117 kcal/mol on primary analysis of docking results. Figs. 3 and 4 show 2D and 3D binding interaction with the pocket boundary and pocket cavity, with the dotted line and active pocket surface of *E. coli* FabH protein residues labelled with their short-code within the radius of 4.20 Å of the ligand atom. The binding energy of compound **7d** and *E. coli* FabH are shown in which three types of interaction present hydrophobic, aromatic interactions and cationic-pi interaction with the aromatic ring. The binding was stabilized by one pi-pi interaction between Trp 32 and the methoxy phenyl ring adjacent to the pyrazole ring adjacent to the pyrazole ring with a bond distance of 3.49 Å. Pyrazole forms two hydrogen bonds, the first of which is the hydrogen of Gly 152 and pyrazole ring with a bond distance of 3.67 Å and the second of which is the hydrogen of Arg 151 and pyrazole ring with bond distance 4.75 Å, cation-pi interaction between imidazole and Arg 151 with bond distance 4.75 Å in the form of arene hydrogen interaction. From this interaction and the binding score, it can be primarily concluded that the strong hydrogen bonding, pi-pi interaction and cationic-pi interaction by the pyrazole ring, imidazole ring and methyl phenyl ring fragment with Trp 32, Gly 152 and Arg 151 is responsible for the effective FabH inhibitory of compound **7d** in docking results.

Computational studies

Density functional theory: The structural geometry of all the synthesized compounds **7a-h** was optimized to their minimum possible energy level using the quantum computational

TABLE-4
BINDING ENERGY OF COMPOUNDS **7a-h** WITH FabH

Compd.	R ₁	R ₂	Binding energy (ΔG_b)
7a	H	H	-7.6056
7b	H	CH ₃	-7.5064
7c	CH ₃	H	-7.7224
7d	CH ₃	CH ₃	-8.9117
7e	OCH ₃	H	-7.9413
7f	OCH ₃	CH ₃	-8.1580
7g	Cl	H	-7.7091
7h	Cl	CH ₃	-7.8443

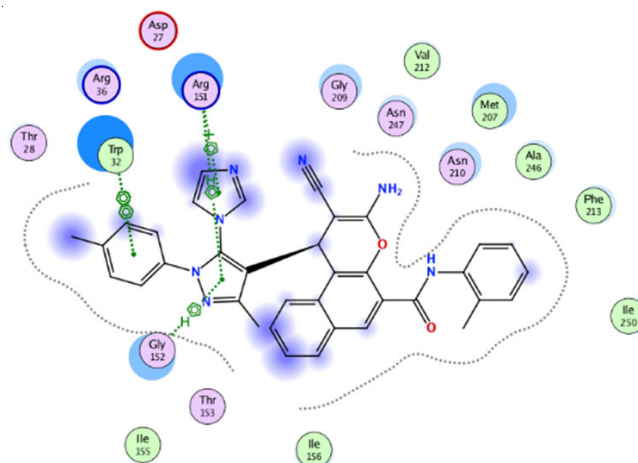


Fig. 3. 2D Binding model of compound **7d** into the active pocket of FabH

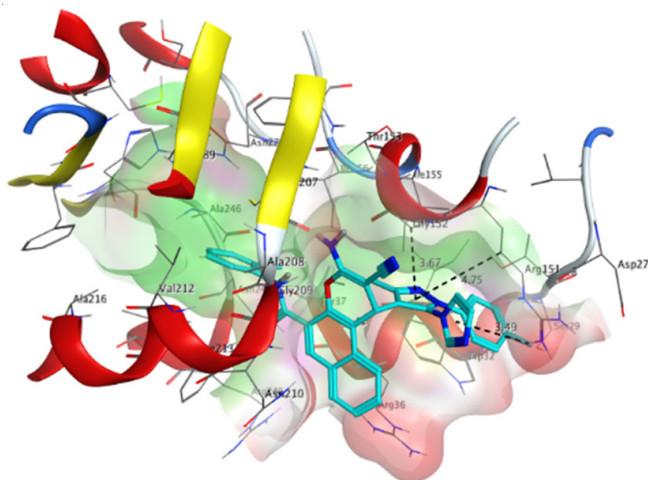


Fig. 4. 3D Binding model of compound **7d** into the active pocket of FabH

tool ORCA 5.0.3 with the DFT method and B3LYP level of DFT theory and def-2SVP basis set [25,26]. The output structures with the minimum energy of the synthesized compounds **7a-h** were analyzed for the IR frequency range, none of them were found with the negative vibrational frequency of the optimized structure and hence the lowest frequency value of the output structure was preferred for the geometry study. The influence of substitution groups changing R₁ and R₂ positions on the geometry of molecules was studied by using density functional theory (DFT). Based on the potential planarity of the optimized compound, two main cores of atoms **7a-h** were

found, so that two imaginary planes were passed through atoms, where the first plane was passed from imidazole ring having R_1 substitution and the second plane was passed from benzo-chromene core having R_2 substitution, therefore in compounds **7a-h** there is only one twist angle θ . It was conventional that the smaller the molecular orbital energy gap ΔE , the greater the reactivity and lower kinetic stability of the materials, but from recent work we know that this conventional relation is

not obeyed in all the cases [27-29]. The factors calculated from the quantum computational DFT study of all the compounds **7a-h** are shown in Table-5. The highest occupied molecular orbital (HOMO) and least unoccupied molecular orbital (LUMO) of all the synthesized compounds are represented in the molecular surface plot in Fig. 5. It can be observed that in molecules **7a** to **7h**, the HOMO density delocalized is spread over the imidazole and pyrazole moiety of the molecule but in molecules

TABLE-5
FACTORS CALCULATED FROM THE QUANTUM COMPUTATIONAL DFT STUDY OF MOLECULES **7a-h**

Element	7a	7b	7c	7d	7e	7f	7g	7h
Dipole moment (Debye)	1.939	4.235	2.209	1.958	3.512	3.234	2.176	1.613
Energy (a.u.)	-1841.960	-1881.220	-1881.220	-1920.476	-1956.338	-1995.594	-2301.363	-2340.619
Twist angle (θ)	24.24	24.54	24.77	22.91	25.04	23.12	25.16	22.85
E_{HOMO} (eV)	-10.133	-10.161	-10.130	-10.121	-10.118	-10.109	-10.098	-10.090
E_{LUMO} (eV)	-4.397	-3.767	-4.392	-4.215	-4.395	-4.217	-4.390	-4.210
$I = -E_{\text{HOMO}}$	10.133	10.161	10.130	10.121	10.118	10.109	10.098	10.090
$A = -E_{\text{LUMO}}$	4.397	3.767	4.392	4.215	4.395	4.217	4.390	4.210
$\Delta E = I - A$ (eV)	5.736	6.394	5.738	5.906	5.723	5.892	5.708	5.880
$\eta = (I - A)/2$	2.868	3.197	2.869	2.953	2.862	2.946	2.854	2.940
$\chi = (I + A)/2$	7.265	6.964	7.261	7.168	7.257	7.163	7.244	7.150
$\sigma = 1/\eta$	0.349	0.313	0.349	0.339	0.349	0.339	0.350	0.340
$S = 1/2\eta$	0.174	0.156	0.174	0.169	0.175	0.170	0.175	0.170
$\Pi = -\chi$	-7.265	-6.964	-7.261	-7.168	-7.257	-7.163	-7.244	-7.150
$\omega = (\Pi)^2/2\eta$	9.202	7.585	9.188	8.700	9.201	8.708	9.193	8.694
$\Delta N_{\text{max}} = \chi/\eta$	2.533	2.178	2.531	2.427	2.536	2.431	2.538	2.432

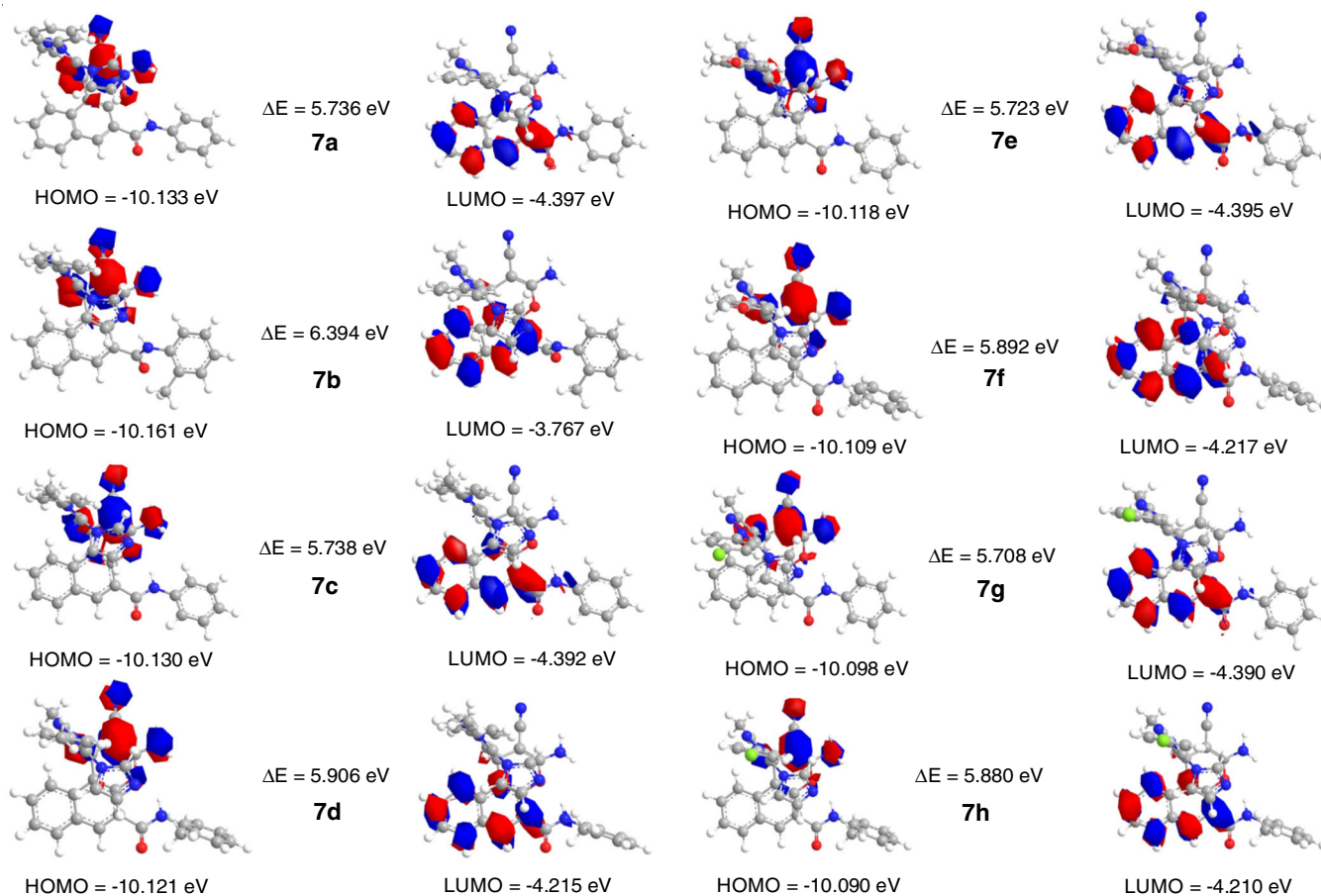


Fig. 5. Frontier molecular orbitals diagram of **7a-h**

7e to **7h**, the HOMO density is shifted to R₁ substituted phenyl ring due to the more electron negative groups. The LUMO density is spread over the benzochromene core of the molecule, while no such change is seen in the benzochromene core of the molecule due to the R₂ substituted. Parameters based on the molecular orbital energy and their energy gap are also calculated where they can be used to relate them with other molecular properties of the ligand such parameters as softness, hardness, global softness, absolute softness, chemical potential, global electrophilicity, electronegativity and additional electronic charge are reported in Table-5 with the molecular energy, twist angles between planes and dipole moment. It was conventional that the softness is directly related to the biological activity of the ligand, but the biological activity data obtained it can be said that the data in Table-5 are not sufficient to predict the reactivity of the molecules.

Molecular docking study: The inhibition of EGFR kinase and antiproliferative activity IC₅₀ (μM) of compounds **7a-h** is reported in Table-1, it was observed that among all the compounds, compound **7e** exhibited greater potency against all three cancer cell lines, which are EGFR, A549 and HepG2 with the IC₅₀ of 12.23 ± 0.04, 19.54 ± 0.02 and 18.23 ± 0.06, respectively. Compound **7a** showed least activity against the EGFR with IC₅₀ of 12.23 ± 0.04, while compound **7b** showed the least activity against A549 cell line with IC₅₀ of 19.54 ± 0.02 and compound **7a** showed the least activity against HepG2 IC₅₀ of 18.23 ± 0.06, this can be attributed to the nature of the substituents in conjugation with the core of the molecule, the higher activity of the molecule can be due to the presence of hydrogen at R₁ and R₂, this position can be a good hydrogen bond acceptor. While in the least active molecules, the presence of the -CH₃ group at all the substitution positions can only

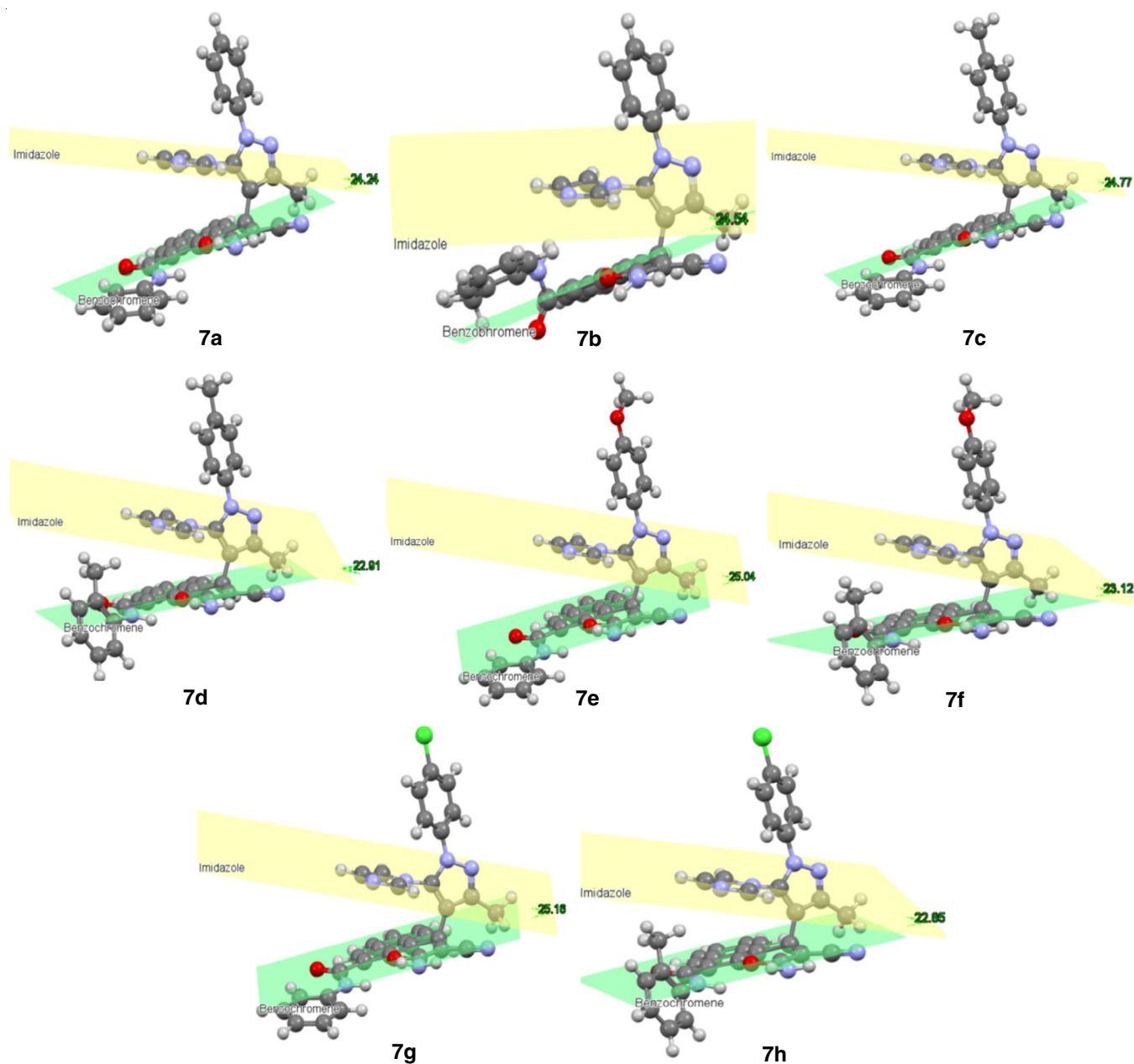


Fig. 6. Twist angle θ of **7a-h**

increase the electron density in the core, which must be binding with the pocket least firmly compared to all others. The change in the substitution can affect the geometry of the molecule also which is a critical factor in protein binding hence this change can bring a change in the twist angle between the aromatic part of the molecule allowing the molecule to fit perfectly or adversely in the pocket of EGFR, which can be quantitatively seen in Table-5, also qualitatively it can be observed in Fig. 6. The stronger biological interaction of compound **7f** with the protein is with residue Arg 817, where it forms one hydrogen bond between π -electron of methoxy phenyl ring and hydrogen of Arg 817 with a bond distance of 3.18 Å with the binding energy of -7.5749 kcal/mol. This interaction of compound **7f** with protein residues is shown in Fig. 7. In case of FabH *E. coli*, the inhibition concentration data for all the prepared compounds shows that compound **7d** exhibited greater potency with the IC₅₀ concentration of 3.4 μ M, while compound **7b**

showed the least potency against *E. coli* with the IC₅₀ concentration of 18.2 μ M, from the docking score it can be seen that compound **7d** bound with the least binding energy with the protein and their interaction in 2D and 3D shown in Fig. 8.

Conclusion

This study aimed to synthesize new molecules with imidazole-pyrazole-benzo[f]chromene hybrids for their potential against lung and breast cancer. Eight derivatives were synthesized with smaller groups at substitution positions. The synthesized compounds **7a-h** were aimed for their anticancer antimicrobial activity and some significant biological results were obtained with a conclusion that when imidazole-pyrazole and methyl/methoxy substitution at the R₁ position is present in the molecules, its hydrogen and the phenyl ring bind with the protein and enhances the binding with more affinity also, the imidazole-pyrazole-benzo[f]chromene core with electron-

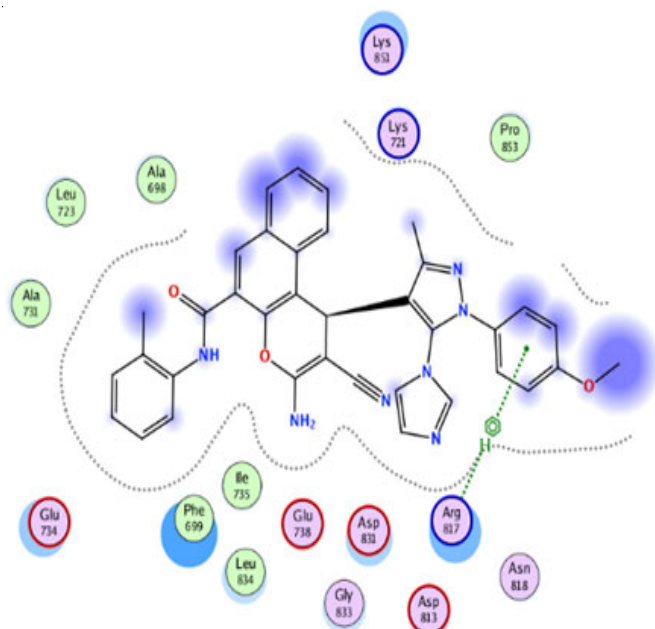


Fig. 7. 2D & 3D Binding model of compound **7f** into the active pocket of EGFR

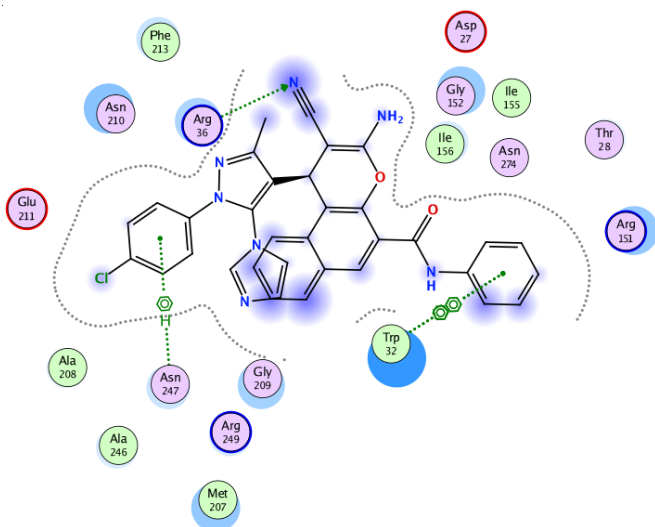
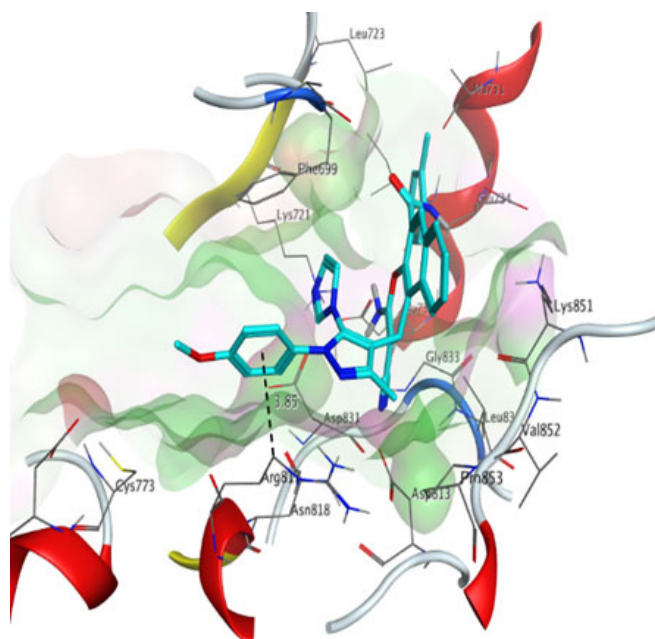
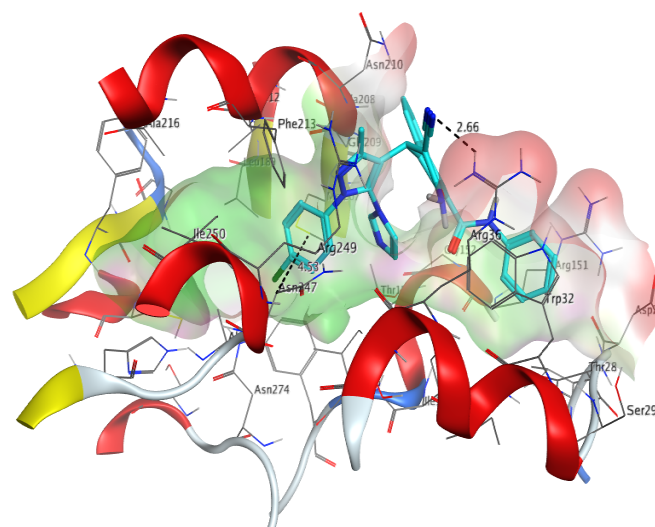


Fig. 8. 2D & 3D Binding model of compound **7h** into the active pocket of FabH



donating and hydrogen bond acceptor plays a major role in fitting the active pocket of protein. Compound **7f** was shown to be the most active against EGFR, A549 and HepG2 cancer cell lines, while compound **7h** showed to be the most active against FabH *E. coli*, although other members of the prepared series were also found to be active with comparatively higher inhibition concentration. The highest inhibition power of the potent prepared derivative against EGFR was about fourth time lower than the taken standard, while for A549 the potency was seventeenth time lower than the standard. To understand the binding posture and sites, the molecular docking was performed. Compound **7e** was bound into the active site of EGFR pocket with the minimum binding energy of $\Delta G_b = -7.6894$ kcal/mol, compound **7d** was bound into the active site of FabH pocket with the minimum binding energy of $\Delta G_b = -8.9117$ kcal/mol, amongst the all docked amongst the all docked. From this study and observation, it can be concluded that molecules with imidazole-pyrazole and broader molecular core composed of benzo[*f*]chromene pharmacophores can be used as templet and can be further structurally modified for target-based application, evaluating the further scope of the pharmacophore and study the limitations that cannot be explored by *in vitro* is further needed.

ACKNOWLEDGEMENTS

The authors are thankful to Shri Maneklal M. Patel Institute of Sciences and Research, Kadi Sarva Vishwavidhyalaya, Gandhinagar for giving infrastructure and laboratory facilities.

CONFLICT OF INTEREST

The authors declare that there is no conflict of interests regarding the publication of this article.

REFERENCES

1. T.S. Ibrahim, M.M. Hawwas, E. Taher, N.A. Alhakamy, M.A. Alfaleh, M. Elagawany, B. Elgendy, G.M. Zayed, M.F.A. Mohamed, Z.K. Abdel-Samii and Y.A.M.M. Elshaier, *Bioorg. Chem.*, **105**, 104352 (2020); <https://doi.org/10.1016/j.bioorg.2020.104352>
2. R.L. Siegel, K.D. Miller, H.E. Fuchs and A. Jemal, *CA Cancer J. Clin.*, **71**, 7 (2021); <https://doi.org/10.3322/caac.21654>
3. M. Morales-Cruz, Y. Delgado, B. Castillo, C.M. Figueroa, A.M. Molina, A. Torres, M. Milián and K. Griebenow, *Drug Des. Devel. Ther.*, **13**, 3753 (2019); <https://doi.org/10.2147/DDDT.S219489>
4. M. Tateishi and T. Ishida, *Cancer Res.*, **50**, 7077 (1990).
5. A. Ayati, S. Moghimi, S. Salarinejad, M. Safavi, B. Pouramiri and A. Foroumadi, *Bioorg. Chem.*, **99**, 103811 (2020); <https://doi.org/10.1016/j.bioorg.2020.103811>
6. S.W. White, J. Zheng, Y.M. Zhang and C.O. Rock, *Annu. Rev. Biochem.*, **74**, 791 (2005); <https://doi.org/10.1146/annurev.biochem.74.082803.133524>
7. K.S. Kolibaba and B.J. Druker, *Biochim. Biophys. Acta*, **1333**, F217 (1997); [https://doi.org/10.1016/s0304-419x\(97\)00022-x](https://doi.org/10.1016/s0304-419x(97)00022-x)
8. E.J. Meuillet and E.G. Bremer, *Pediatr. Neurosurg.*, **29**, 1 (1998); <https://doi.org/10.1159/000028677>
9. M.C. Mandewale, U.C. Patil, S.V. Shedde, U.R. Dappadwad and R.S. Yamgar, *Beni. Suef Univ. J. Basic Appl. Sci.*, **6**, 354 (2017); <https://doi.org/10.1016/j.bjbas.2017.07.005>
10. R. Kaur and K. Kumar, *Eur. J. Med. Chem.*, **215**, 113220 (2021); <https://doi.org/10.1016/j.ejmech.2021.113220>
11. F. Zhang, Q. Wen, S.-F. Wang, B. Shahla Karim, Y.-S. Yang, J.-J. Liu, W.-M. Zhang and H.-L. Zhu, *Bioorg. Med. Chem. Lett.*, **24**, 90 (2013); <https://doi.org/10.1016/j.bmcl.2013.11.079>
12. Y.-J. Lu, Y.-M. Zhang and C.O. Rock, *Biochem. Cell Biol.*, **82**, 145 (2004); <https://doi.org/10.1139/o03-076>
13. Y.-T. Wang, T.-Q. Shi, J. Fu and H.-L. Zhu, *Eur. J. Med. Chem.*, **171**, 209 (2019); <https://doi.org/10.1016/j.ejmech.2019.03.026>
14. A. Mermer, T. Keles and Y. Sirin, *Bioorg. Chem.*, **114**, 105076 (2021); <https://doi.org/10.1016/j.bioorg.2021.105076>
15. J. Drogosz-Stachowicz, A. Dlugosz-Pokorska, K. Gach-Janczak, A. Jaskulska, T. Janecki and A. Janecka, *Chem. Biol. Interact.*, **320**, 109005 (2020); <https://doi.org/10.1016/j.cbi.2020.109005>
16. Z. Xiao, F. Lei, X. Chen, X. Wang, L. Cao, K. Ye, W. Zhu and S. Xu, *Arch. Pharm.*, **351**, 1700407 (2018); <https://doi.org/10.1002/ardp.201700407>
17. D. Mantu, V. Antoci, C. Moldoveanu, G. Zbancioc and I.I. Mangalagiu, *J. Enzyme Inhib. Med. Chem.*, **31**(Suppl.2), 96 (2016); <https://doi.org/10.1080/14756366.2016.1190711>
18. A. Irfan, F. Batool, S.A. Zahra Naqvi, A. Islam, S.M. Osman, A. Nocentini, S.A. Alissa and C.T. Supuran, *J. Enzyme Inhib. Med. Chem.*, **35**, 265 (2020); <https://doi.org/10.1080/14756366.2019.1698036>
19. Haroun, C. Tratrati, K. Kositzi, E. Tsolaki, A. Petrou, B. Aldhubiab, M. Attimarad, S. Harsha, A. Geronikaki, K.N. Venugopala, H.S. Elsewedy, M. Sokovic, J. Glamoclija and A. Ciric, *Curr. Top. Med. Chem.*, **18**, 75 (2018); <https://doi.org/10.2174/1568026618666180206101814>
20. N.C. Desai, D. Pandya and D. Vaja, *Med. Chem. Res.*, **27**, 52 (2018); <https://doi.org/10.1007/s00044-017-2040-5>
21. R. Ali and N. Siddiqui, *J. Chem.*, **2013**, 345198 (2013); <https://doi.org/10.1155/2013/345198>
22. Singh, A. Pandurangan, K. Rana, P. Anand, A. Ahamad and A.K. Tiwari, *Int. Curr. Pharm. J.*, **1**, 110 (2012); <https://doi.org/10.3329/icpj.v1i5.10284>
23. W.H. Mahmoud, M.M. Omar, F.N. Sayed and G.G. Mohamed, *Appl. Organomet. Chem.*, **32**, 4386 (2018); <https://doi.org/10.1002/aoc.4386>
24. R. Kurtaran, S. Odabasioglu, A. Azizoglu, H. Kara and O. Atakol, *Polyhedron*, **26**, 5069 (2007); <https://doi.org/10.1016/j.poly.2007.07.021>
25. F. Neese, *Wiley Interdiscip. Rev. Comput. Mol. Sci.*, **2**, 73 (2012); <https://doi.org/10.1002/wcms.81>
26. F. Neese, *Wiley Interdiscip. Rev. Comput. Mol. Sci.*, **8**, e1327 (2018); <https://doi.org/10.1002/wcms.1327>
27. P. Sharma, R. Patel, R.R. Koshti, A. Vyas and C.B. Sangani, *Asian J. Chem.*, **35**, 1320 (2023); <https://doi.org/10.14233/ajchem.2023.27650>
28. R. Patel, P. Sharma, R.R. Koshti, A. Vyas and C.B. Sangani, *Asian J. Chem.*, **35**, 1616 (2023); <https://doi.org/10.14233/ajchem.2023.27921>
29. P. Sharma, R. Patel, R.R. Koshti, A. Vyas and C.B. Sangani, *Asian J. Chem.*, **35**, 2092 (2023); <https://doi.org/10.14233/ajchem.2023.28081>